Accurate tight-binding models for the π bands of bilayer graphene

Jeil Jung
Department of Physics, University of Texas at Austin, Austin, Texas 78712-0264, USA
and Department of Physics, National University of Singapore, Singapore

Allan H. MacDonald
Department of Physics, University of Texas at Austin, Austin, Texas 78712-0264, USA
(Received 20 September 2013; revised manuscript received 12 December 2013; published 6 January 2014)

We derive an *ab initio* π-band tight-binding model for AB stacked bilayer graphene based on maximally localized Wannier wave functions centered on the carbon sites, finding that both intralayer and interlayer hopping is longer in range than assumed in commonly used phenomenological tight-binding models. Starting from this full tight-binding model, we derive two effective models that are intended to provide a convenient starting point for theories of π-band electronic properties by achieving accuracy over the full width of the π bands, and especially at the Dirac points, in models with a relatively small number of hopping parameters. The simplified models are then compared with phenomenological Slonczewski-Weiss-McClure–type tight-binding models in an effort to clarify confusion that exists in the literature concerning tight-binding model parameter signs.

DOI: 10.1103/PhysRevB.89.035405 PACS number(s): 73.22.Pr, 71.20.Gj, 71.15.Mb, 31.15.aq

I. INTRODUCTION

π bands are responsible for the low-energy electronic properties of graphitic systems, including single and multilayer graphene. It is often convenient to base theories of electronic properties on orthogonal orbital tight-binding models similar to the Slonczewski-Weiss-McClure [1–3] (SWM) π-band tight-binding model used extensively in graphite. The most important parameters in these models are the near-neighbor hopping amplitude within the graphene layers, which sets the π-band width, and the near-neighbor interlayer hopping amplitude which partially splits [4] the two states per layer which are nearly degenerate at the Brillouin-zone corner points K and K'. Although smaller in magnitude other parameters still play a crucial role in determining electronic properties in multilayer graphene systems, for example, by moving level crossings (Dirac points) away from K and K', and cannot be guessed with sufficient accuracy simply by making analogies with the graphite case. In this paper we attempt to achieve a broader perspective on these tight-binding models by deriving a π-band model for bilayer graphene from *ab initio* electronic structure calculations. Bilayer graphene is the simplest multilayer system and can be viewed as an isolated copy of the two-layer repeating unit of Bernal or AB stacked graphite. Tight-binding models for bilayer graphene have been proposed previously based on analogies to the SWM model for graphite [5,6], on phenomenological fits to Raman [7] and infrared [8,9] measurements, and on parametric fits to first principles bands [10,11]. Our work differs from previous analyses because it is based on a direct calculation of tight-binding model parameters, rather than on an ill-conditioned fitting procedure. This approach provides a model in which both wave-function character and band energies are accurately represented, provides a more complete physical picture of π-band electronic structure, and resolves some inconsistencies between models that have been proposed in earlier work.

The literature on tight-binding models for bilayer graphene does not provide consistent magnitudes or even signs for the small remote hopping parameters that reshape the bands near the Dirac points. In this paper we obtain π-band tight-binding models from first principles LDA electronic structure calculations combined with maximally localized Wannier functions (MLWF) centered at the carbon sites [12]. Models based on Wannier functions with well defined symmetries benefit from the orthonormality of the localized orbitals and give rise to matrix elements that can be physically interpreted as hopping between π orbitals centered on different sites. A π-band only model for bilayer graphene should be accurate because hybridization between π and σ orbitals is weak in all multilayer graphene systems [13,14]. Calculations based on the LDA have the advantage that they do not incorporate the many-body band renormalizations due to screened nonlocal exchange that are known to be important in graphene and multilayer graphene systems. The resulting bands can therefore be used as a starting point for studies of many-body band renormalization, as is common practice for example in GW approximations calculations [15].

The present work extends a previous analysis carried out for single-layer graphene [16], to the case of Bernal stacked bilayer graphene. The Hamiltonian we obtain provides an intuitive understanding of remote hopping processes both within and between layers. One important finding is that both intralayer and interlayer hopping processes have longer range than assumed in phenomenological tight-binding models. We therefore propose a systematic scheme which we use to obtain alternate effective tight-binding models with a smaller number of parameters which retain both accuracy near Dirac points and a good description of the full π bands. Our paper is structured as follows. In Sec. II we summarize the full tight-binding (FTB) model of bilayer graphene's π bands obtained from a calculation that constructs maximally localized Wannier functions. In Sec. III we explain the relationship between tight-binding and continuum models and the scheme used

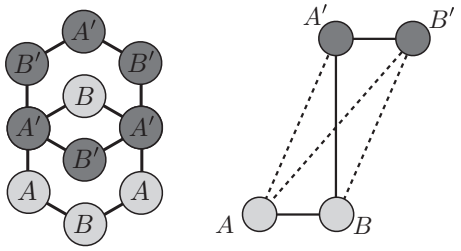

FIG. 1. Definition of the unit cell for Bernal or AB stacked bilayer graphene. The A' site of the top layer sits right above a B site of the lower layer. The A and B' sites do not have a corresponding vertical neighbor. The solid lines in the right panel represent the large-amplitude hopping processes in literature tight-binding models, whereas the dotted lines indicate weaker processes that are responsible for particle-hole symmetry breaking and trigonal distortions. In the main text we quantify the role they play in bilayer graphene electronic structure.

to derive the simplified tight-binding models which we hope will be a convenient starting point for some π-band electronic property theories. We then devote Sec. IV to a comparison between our simplified models and models that have been used in the literature for bilayer graphene systems. Finally our conclusions are summarized in Sec. V.

II. WANNIER INTERPOLATION OF BERNAL BILAYER GRAPHENE π BANDS

A π-band model of bilayer graphene contains four orthogonal orbitals per unit cell, corresponding to p_z orbitals centered on the A, B sites in the bottom layer and A' and B' sites in the top layer. We have fixed the lattice constants at the experimental values of graphite for which the in-plane lattice constant is $a = 2.46$ Å and the interlayer separation is $c = 3.35$ Å. Fixing the interlayer separation at the experimental value accounts for the influence of dispersive van der Waals interactions, which are not accurately captured in the LDA. Dispersive interactions are only indirectly related to π-band quasiparticle energies. We label the Bernal (AB) stacked honeycomb lattice sites so that the A' site on the top layer is directly above the B site in the bottom layer as illustrated in Fig. 1. Our definitions of the in-plane lattice vectors and Bloch functions are similar to those used in Ref. [16] for single-layer graphene and are also presented in Appendix A. The technical details of the calculations used to extract the Wannier functions are also similar to those of the single-layer case. We used the plane-wave first principles calculation package QUANTUM ESPRESSO [17] and WANNIER90 [18] to construct the Wannier functions. The QUANTUM ESPRESSO calculations used the Perdew-Zunger parametrization [19] of the local density approximation [20]. The tight-binding model parameters obtained using a 30×30 k-space sampling density are listed in Appendix B. Band structures resulting from Wannier interpolation for two different k-point sampling densities are presented in Fig. 2 where we show the excellent agreement between the tight-binding model and the first principle calculation for 30×30 sampling, indicating that the parameters for hopping processes more remote that those listed in Appendix B are entirely negligible.

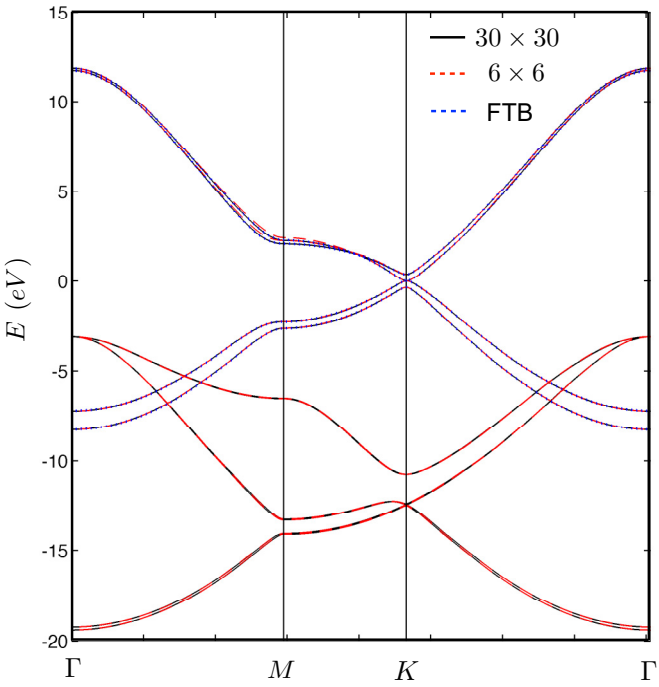

FIG. 2. (Color online) Band structure of AB stacked bilayer graphene obtained through Wannier interpolation of first principles LDA results for 6×6 and 30×30 k-point sampling densities. The 6×6 interpolation is accurate except near the M point, where the maximum deviation is ~ 0.2 eV, and the 30×30 interpolation is accurate throughout the Brillouin zone. The difference near the M point between the 6×6 and 30×30 Wannier interpolation is larger than in the single-layer graphene case.

The π-band Hamiltonian for bilayer graphene is a $\mathbf{k}$-dependent four dimensional matrix:

$$H(\mathbf{k}) = \begin{pmatrix} H_B(\mathbf{k}) & H_{BT}(\mathbf{k}) \\ H_{TB}(\mathbf{k}) & H_T(\mathbf{k}) \end{pmatrix}, \tag{1}$$

where $H_B(\mathbf{k})$ and $H_T(\mathbf{k})$ are two dimensional matrices that describe intra- and intersublattice hopping within the bottom and top graphene layers. The Hamiltonian of the bottom graphene sheet is

$$H_B(\mathbf{k}) = \begin{pmatrix} H_{AA}(\mathbf{k}) & H_{AB}(\mathbf{k}) \\ H_{BA}(\mathbf{k}) & H_{BB}(\mathbf{k}) \end{pmatrix}, \tag{2}$$

and the Hamiltonian of the top graphene sheet

$$H_T(\mathbf{k}) = \begin{pmatrix} H_{A'A'}(\mathbf{k}) & H_{A'B'}(\mathbf{k}) \\ H_{B'A'}(\mathbf{k}) & H_{B'B'}(\mathbf{k}) \end{pmatrix}. \tag{3}$$

Both intralayer and interlayer hopping processes can be classified into symmetry equivalent groups. The grouping of intralayer processes is identical to that in single-layer graphene [16]. The intralayer Hamiltonian can be written as a sum over groups of the product of a hopping strength for the

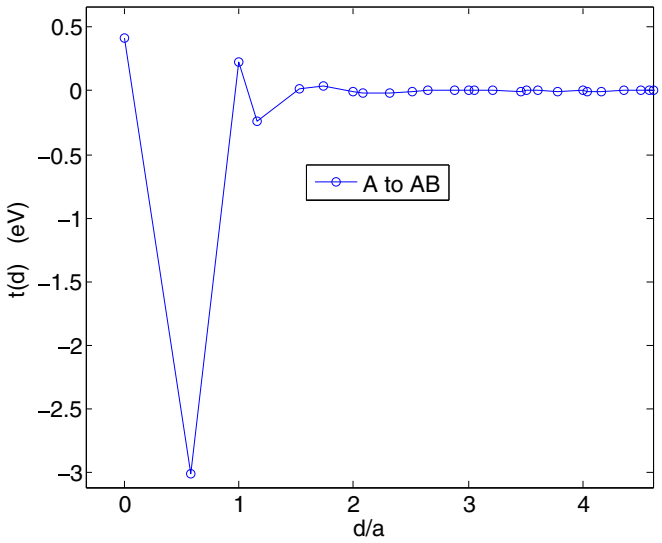

FIG. 3. (Color online) Intralayer hopping terms in Bernal bilayer graphene evaluated starting from A to A and B sites in the bottom layer with 30×30 k-point sampling density. The intralayer Hamiltonian matrix elements are extremely similar to those of isolated graphene layers obtained in Ref. [16] in spite of the interlayer coupling effect. The difference between isolated layer and bilayer intralayer hopping is not visible on the scale of this figure.

group and a structure factor:

$$H_{A(')B(')}(\mathbf{k}) = \sum_n t_{A(')B(')n} f_n(\mathbf{k}), \tag{4}$$

$$H_{B(')A(')}(\mathbf{k}) = \sum_n t_{B(')A(')n} f_n^*(\mathbf{k}), \tag{5}$$

$$H_{A(')A(')}(\mathbf{k}) = \sum_n t'_{A(')A(')n} g_n(\mathbf{k}), \tag{6}$$

$$H_{B(')B(')}(\mathbf{k}) = \sum_n t'_{B(')B(')n} g_n(\mathbf{k}). \tag{7}$$

The structure factors $f_n(\mathbf{k})$ and $g_n(\mathbf{k})$ are defined in Ref. [16]. Inversion symmetry leads to the following relations between the hopping amplitudes in top and bottom layers:

$$t_{ABn} = t_{B'A'n}, \quad t'_{AAn} = t'_{B'B'n}, \quad t'_{BBn} = t'_{A'A'n}. \tag{8}$$

The intralayer hopping amplitude values are extremely close to those obtained for isolated graphene layers as summarized in Fig. 3.

Coupling between layers is described by the $H_{BT}(\mathbf{k}) = H^*_{TB}(\mathbf{k})$, where

$$H_{BT}(\mathbf{k}) = \begin{pmatrix} H_{AA'}(\mathbf{k}) & H_{AB'}(\mathbf{k}) \\ H_{BA'}(\mathbf{k}) & H_{BB'}(\mathbf{k}) \end{pmatrix}. \tag{9}$$

We find that

$$H_{AA'}(\mathbf{k}) = \sum_n t_{AA'n} f_n(\mathbf{k}), \tag{10}$$

$$H_{AB'}(\mathbf{k}) = \sum_n t_{AB'n} f_n^*(\mathbf{k}), \tag{11}$$

$$H_{BA'}(\mathbf{k}) = \sum_n t'_{BA'n} g_n(\mathbf{k}), \tag{12}$$

$$H_{BB'}(\mathbf{k}) = \sum_n t_{BB'n} f_n(\mathbf{k}), \tag{13}$$

where the interlayer structure factors are related to intralayer structure factors by $f_n = f_{ABn} = f_{A'B'n} = f_{AA'n} = f^*_{AB'}$ and $g_n = g_{AAn} = g_{BBn} = g_{A'A'n} = g_{B'B'n} = g_{BA'n}$, as is apparent when we compare the lattice sites illustrated in Fig. 4. The interlayer hopping terms are plotted in Fig. 5 as a function of the in-plane projection of the hopping distances. Two hopping terms are prominent but, as we will discuss later on, smaller terms do play a role in defining details of the electronic structure both near and far away from the Dirac point.

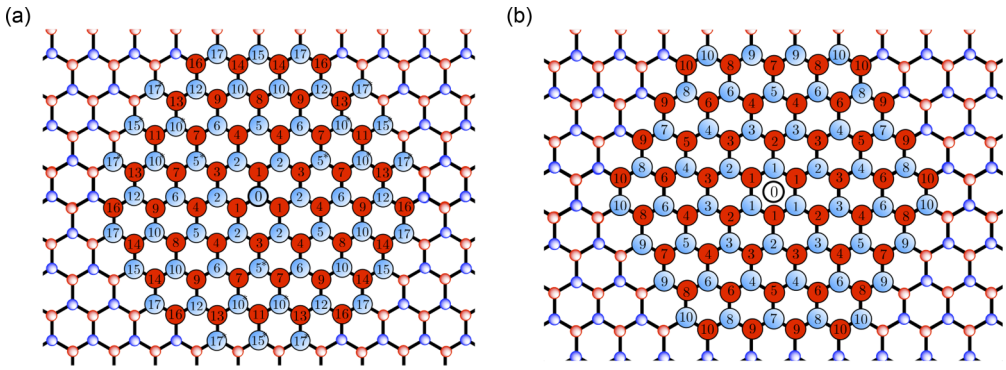

FIG. 4. (Color online) Neighbor classification relative to a central reference point labeled 0. Neighbors of a given site can be grouped into symmetry equivalent subsets with identical hopping parameters. The neighbor groups are ordered by their distance from the reference point. mth nearest neighbors of the reference point are labeled in this figure by the integer m. *Left panel:* Neighbor classifications for intralayer AB pairs and for interlayer BA' and BB' pairs. *Right panel:* Neighbor classification for interlayer AA', AB' pairs. The structure factors (see text) in AA' matrix elements are identical to those in AB elements. The structure factors in AB' acquire a mirror reflection in the y direction that leads to a complex conjugation in the matrix elements. The integer labels are derived by grouping neighbors according to in-plane separation so that some AA' and AB' neighbor pairs share labels with pairs in the left panel.

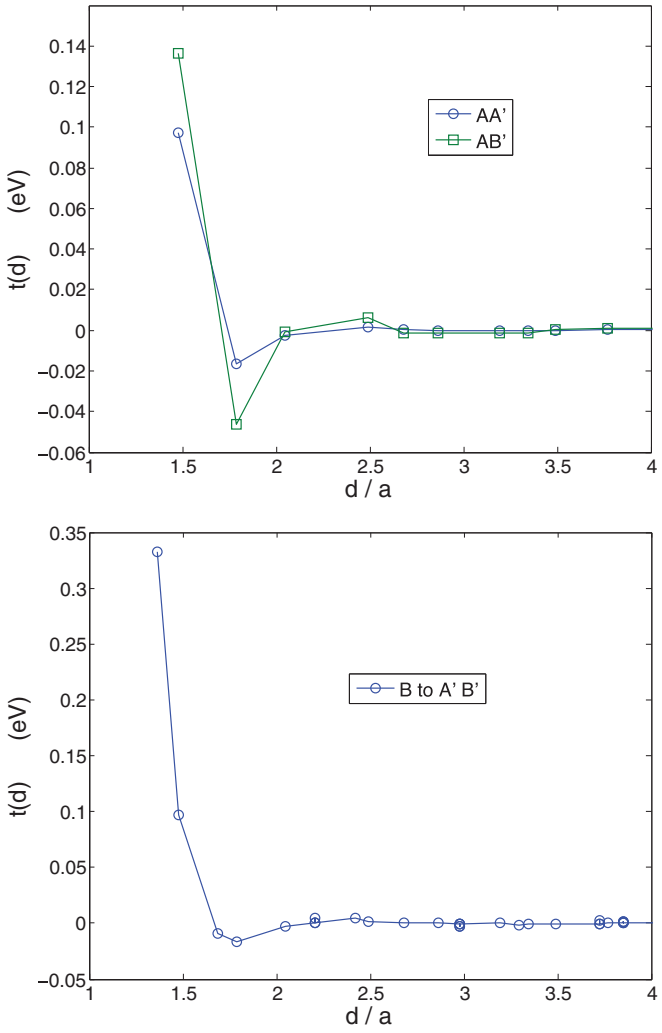

FIG. 5. (Color online) *Upper panel:* Hopping parameters connecting site A of the bottom layer to the A' and B' sites in the top layer. The distances on the horizontal axis correspond to in-plane projections of displacements. *Lower panel:* Hopping parameters connecting site B of the bottom layer to the top layer sites. Note that two different values occur for some values of d ($m = 5,10,15,17$) because of the occurrence of neighbor pairs which share the same projected displacements that are not symmetry equivalent. These cases are marked with an $*$ symbol in Fig. 4.

III. SIMPLIFIED EFFECTIVE MODELS WITH FEWER PARAMETERS

Our maximally localized Wannier function calculations demonstrate that the number of important interlayer hopping processes in few layer graphene systems, and by implication also in graphite, is larger than in SWM-inspired phenomenological models. These phenomenologies provide a good description of states near the Dirac point, but should not be taken literally as a statement concerning the relative strengths of different microscopic processes on an atomic length scale. In the following we discuss the construction of models that are partially in the SWM spirit, in the sense that they concentrate on accuracy near the Dirac point, but are informed by the full maximally localized Wannier function calculation. For this purpose we first carefully discuss the Dirac-point low-energy continuum model implied by particular tight-binding models.

A. Continuum model near the Dirac point

We write the four dimensional π-band Hamiltonian in the form

$$H(\mathbf{k}) = \begin{pmatrix} G_{AA}(\mathbf{k}) & F_{AB}(\mathbf{k}) & F_{AA'}(\mathbf{k}) & F^*_{AB'}(\mathbf{k}) \\ & G_{BB}(\mathbf{k}) & G_{BA'}(\mathbf{k}) & [F_{AA'}(\mathbf{k})] \\ \vdots & \ddots & [G_{BB}(\mathbf{k})] & [F_{AB}(\mathbf{k})] \\ & \cdots & & [G_{AA}(\mathbf{k})] \end{pmatrix}, \tag{14}$$

where we have labeled the Hamiltonian matrix elements by the letters F and G to emphasize that they consist of sums of the f_n and g_n structure factors, respectively. The matrix elements surrounded by square brackets are equivalent to other matrix elements by the symmetry relations $F_{BB'}(\mathbf{k}) = F_{AA'}(\mathbf{k})$, $F_{A'B'}(\mathbf{k}) = F_{AB}(\mathbf{k})$, $G_{A'A'}(\mathbf{k}) = G_{BB}(\mathbf{k})$, and $G_{B'B'}(\mathbf{k}) = G_{AA}(\mathbf{k})$. We discuss all the inequivalent Hamiltonian matrix elements below. Note that $F_{\alpha\beta}(\mathbf{k}_D) = 0$, that the intralayer nonzero values of $G_{\alpha\beta}(\mathbf{k}_D)$ can be interpreted as site energy shifts, and that the interlayer nonzero values of $G_{\alpha\beta}(\mathbf{k}_D)$ can be interpreted as interlayer tunneling amplitudes. The nonzero values of $G_{\alpha\beta}(\mathbf{k}_D)$ play the most essential role in defining the low-energy physics of bilayers. We choose our zero of energy so that $G_{AA}(\mathbf{k}_D) = G_{B'B'}(\mathbf{k}_D) = 0$.

The matrix elements can be expanded up to quadratic order using Eqs. (11)–(16) of Ref. [16]. For $\alpha\beta = AB, AA', BA'$, and wave vectors near $\mathbf{k}_D = (4\pi/3a, 0)$, we write

$$F_{\alpha\beta}(\mathbf{k}_D + \mathbf{q}) \simeq C_{\alpha\beta 1} q\, e^{-i\theta_{\mathbf{q}}} + C_{\alpha\beta 2} q^2 e^{i2\theta_{\mathbf{q}}}. \tag{15}$$

The expansion of the $F_{\alpha\beta}$ functions near $(-4\pi/3a, 0)$ differs by an overall sign and complex conjugation. The dependence of these $\vec{k}\cdot\vec{p}$ Hamiltonian model coefficients on truncation of the full tight-binding model is illustrated in Fig. 6. For $\alpha\beta = AA, BB, BA'$ we write

$$G_{\alpha\beta}(\mathbf{k}_D + \mathbf{q}) \simeq C'_{\alpha\beta 0} + C'_{\alpha\beta 2} q^2. \tag{16}$$

When the small q expansions in Eqs. (15) and (16) are used for the matrix elements of Eq. (14) the electronic structure near the Dirac point is accurately reproduced.

B. Single structure factor tight-binding model

A simplified model that is reminiscent of the Slonczewski-Weiss and McClure (SWM) model for graphite [2] can be constructed by identifying the shortest range hopping model that can capture the correct zeroth order terms in the expansion of $G_{\alpha\beta}(\mathbf{k}_D + \mathbf{q})$ and the correct first order terms in the expansion of $F_{\alpha\beta}(\mathbf{k}_D + \mathbf{q})$. Given a choice for the zero of energy this leaves in a model with five independent parameters:

$$H_{AA}(\mathbf{k}) = H_{BB'}(\mathbf{k}) = t'_{AA0}, \tag{17}$$

$$H_{BB}(\mathbf{k}) = H_{A'A'}(\mathbf{k}) = t'_{BB0}, \tag{18}$$

$$H_{BA'}(\mathbf{k}) = t'_{BA'0} \tag{19}$$

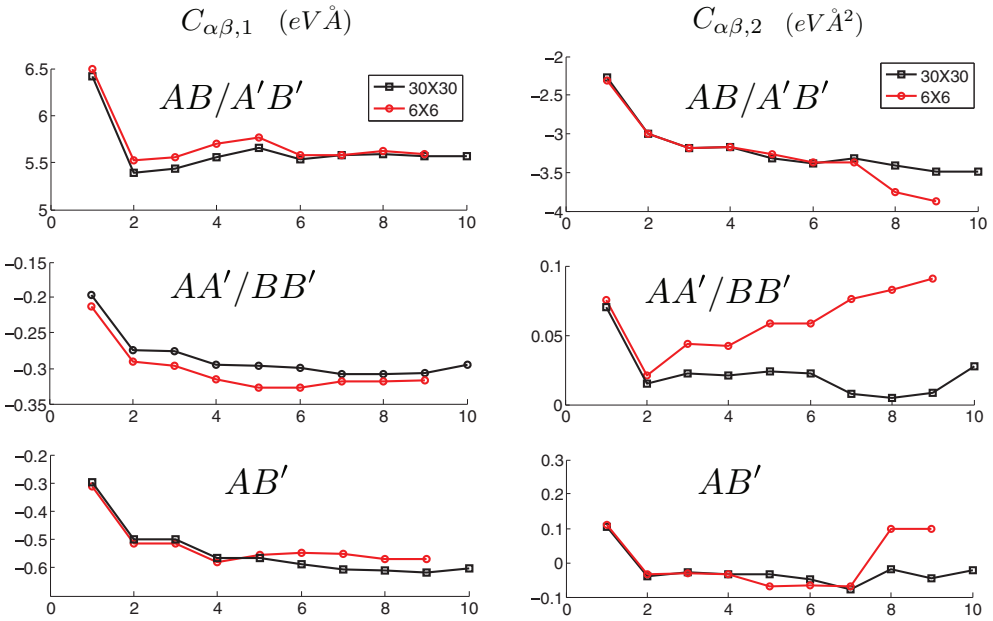

FIG. 6. (Color online) Evolution of the $\vec{k}\cdot\vec{p}$ model coefficients $C_{\alpha\beta1}$ and $C_{\alpha\beta2}$ with neighbor number truncation. These coefficients are used in construction of the effective tight-binding model in Eqs. (20)–(22). The comparison of results obtained by 6×6 and 30×30 calculations points to the need for denser sampling to capture distortions of the local p_z orbitals by interlayer coupling.

and

$$H_{AB}(\mathbf{k}) = H_{A'B'}(\mathbf{k}) = t_{AB1} f_1(\mathbf{k}), \tag{20}$$

$$H_{AA'}(\mathbf{k}) = H_{BB'}(\mathbf{k}) = t_{AA'1} f_1(\mathbf{k}), \tag{21}$$

$$H_{AB'}(\mathbf{k}) = t_{AB'1} f_1^*(\mathbf{k}). \tag{22}$$

Here $f_1(\mathbf{k}) = \exp(ik_y a/\sqrt{3}) + 2\exp(-ik_y a/2\sqrt{3})\cos(k_x a/2)$ with the correct linear dispersion coefficient: with $t_{\alpha\beta1} = -2C_{\alpha\beta,1}/\sqrt{3}a$. The effective tight-binding parameters in this model, listed in Table I, are not the same as the physical hopping parameters listed in the Appendix B. This approximation folds all hopping parameters down to a model with only near-neighbor and on-site or purely vertical type hopping, but has the same continuum model limit as the full tight-binding model. This model achieves accuracy near the Dirac point, and is more accurate across the full Brillouin zone than the continuum model as illustrated in Fig. 7.

TABLE I. $\vec{k}\cdot\vec{p}$ expansion coefficients of the full tight-binding model and parameters of the short-range tight-binding model which reproduces $C'_{\alpha\beta0}$, $C_{\alpha\beta1}$, and $C^{(\prime)}_{\alpha\beta2}$ (see text). Note that $C'_{\alpha\beta0} = t'_{\alpha\beta0}$ and $t_{\alpha\beta1} = -2C_{\alpha\beta1}/\sqrt{3}a$. The units of $t_{\alpha\beta1}$ and $t'_{\alpha\beta0}$ are in eV and the units of $C_{\alpha\beta1}$ and $C^{(\prime)}_{\alpha\beta2}$ are in eV Å and eV Å^2, respectively.

	$F_{\alpha\beta}$				$G_{\alpha\beta}$	
$\alpha\beta$	$t_{\alpha\beta,1}$	$C_{\alpha\beta1}$	$C_{\alpha\beta2}$	$\alpha\beta$	$t'_{\alpha\beta,0}$	$C'_{\alpha\beta2}$
AB, $A'B'$	−2.61	5.567	−3.494	AA	0	−0.269
AA', BB'	0.138	−0.2949	0.0272	BB	0.015	−0.222
AB'	0.283	−0.6036	−0.0227	BA'	0.361	0.103

C. Higher order structure factor models

The accuracy of effective tight-binding models far from the Dirac point can be improved by increasing the number of hopping parameters and associated structure factors. In Ref. [16] for single-layer graphene we saw that a five parameter model with two intersublattice f_n type structure factors and three intrasublattice g_n type structure factors is able to capture both the trigonal distortion of the bands near the Dirac points and particle-hole symmetry breaking throughout the Brillouin zone. One useful recipe to systematically increase the number of parameters in the effective model is to increase the number of structure factors n (and hence the range of the effective tight-binding model) while maintaining correct values for the zeroth and first order $\vec{k}\cdot\vec{p}$ expansion coefficients and also correct values for the strongest shortest range hopping parameters which have a dominant influence on the π-band width. The $n=2$ truncation in the expansions of both the F and G functions leads to what we refer to as the F2G2 model, where we use the correct near-neighbor hopping terms in the Appendix B for the shortest hops and correct the more distant $n=2$ hopping amplitudes using the relations

$$t_{\alpha\beta2} = C_{\alpha\beta1}/\sqrt{3}a + t_{\alpha\beta1}/2, \tag{23}$$

$$t'_{\alpha\beta2} = \tfrac{1}{6}(C'_{\alpha\beta0} - t'_{\alpha\beta0} + 3t'_{\alpha\beta1}) \tag{24}$$

to recover the correct $\vec{k}\cdot\vec{p}$ expansion coefficients. This leads to a fifteen hopping parameter model whose parameters are listed in Table II. The Hamiltonian matrix can be constructed from these parameters using Eqs. (1)–(13). A similar procedure can be applied when we truncate at larger values of n. The overall improvement in the quality of the band structure in the entire Brillouin zone is clearly shown in Fig. 8.

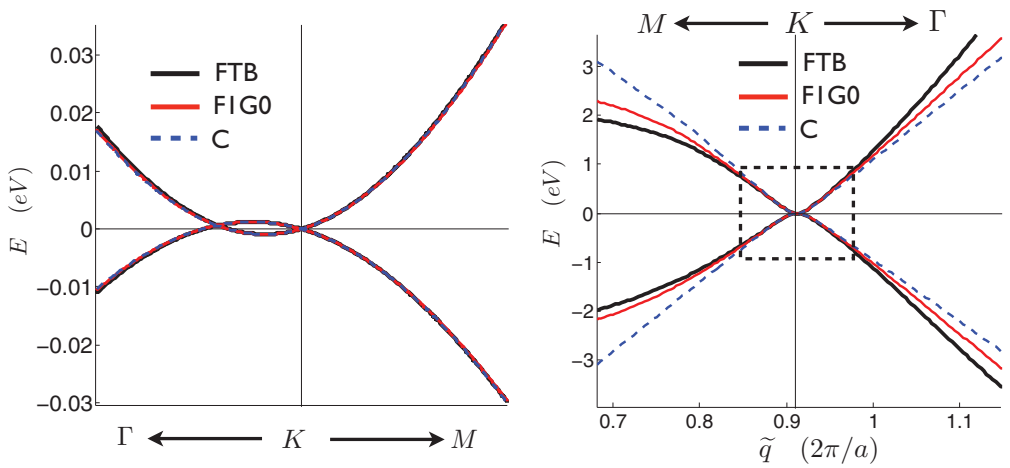

FIG. 7. (Color online) Comparison of electronic structure near the Dirac point for the full tight-binding (FTB) model, the simplified tight-binding model explained in the text (F1G0), and the effective continuum model (C) defined by Eqs. (14)–(16) with the second order term in k neglected. Deviations increase as we move away from the Dirac point, but the relative error is of the order of a few % for $q \sim 1/a$ and F1G0 is superior to the continuum approximation. The dotted square represents the region over which the deviation from the Dirac point $|q| < 1/a$.

IV. TIGHT-BINDING HOPPING AND SWM GRAPHITE MODEL PARAMETERS

It is instructive to compare the tight-binding models discussed in the previous section with bilayer graphene and graphite models used in the literature. Comparison with the SWM model of graphite [2], which has often been used as a guide for band structure parameters in AB stacked few layer graphene systems including Bernal bilayer graphene, is particularly relevant. The SWM model has been popular because of the attractive simplicity of having a reduced set of seven parameters which define the π bands. Partoens and Peeters [5] have made a comparison between tight-binding and SWM model band energies of graphite along two high symmetry lines to obtain equivalence relationships between the parameters of the two models. We use γ_i to designate the SWM parameters. In Appendix C we repeat the analysis in Ref. [5] and find that

$$\begin{aligned} t_0 &\equiv t_{AB1} = -\gamma_0, \quad t_1 \equiv t'_{BA'0} = \gamma_1, \\ t_2 &\equiv t'_{AA''0} = \gamma_2/2, \quad t_3 \equiv t_{AB'1} = \gamma_3, \\ t_4 &\equiv t_{AA'1} = \gamma_4, \quad t_5 \equiv t'_{BB''0} = \gamma_5/2, \\ \Delta' &\equiv t'_{BB0} = \Delta - \gamma_2 + \gamma_5. \end{aligned} \tag{25}$$

TABLE II. Effective hopping parameters in eV units for the F2G2 tight-binding model. (See text.) The $n = 0$ and 1 parameters associated with the f_1, g_0, and g_1 structure factors use the microscopic hopping amplitudes, whereas the hopping terms corresponding to f_2 and g_2 have been adjusted to recover correct values for the $\vec{k} \cdot \vec{p}$ expansion coefficients $C_{1\alpha\beta}$ and $C'_{0\alpha\beta}$.

	t_{ABn}	$t_{AA'n}$	$t_{AB'n}$
f_1	−3.010	0.09244	0.1391
f_2	−0.1984	−0.02299	−0.07211
	t'_{AAn}	t'_{BBn}	$t'_{BA'n}$
g_0	0.4295	0.4506	0.3310
g_1	0.2235	0.2260	−0.01016
g_2	0.04016	0.0404	0.0001

We have defined a new notation for our tight-binding hopping parameters above to facilitate comparison with the SWM model parameters. (Note that the notation $\Delta = \gamma_6$ is used in some papers.) Even though $\gamma_2 = \gamma_5 = 0$ in bilayer graphene we considered a fictitious third layer with ABA stacking order whose sites are labeled with A'' and B'' to complete the equivalence relations between the SWM and the simplified

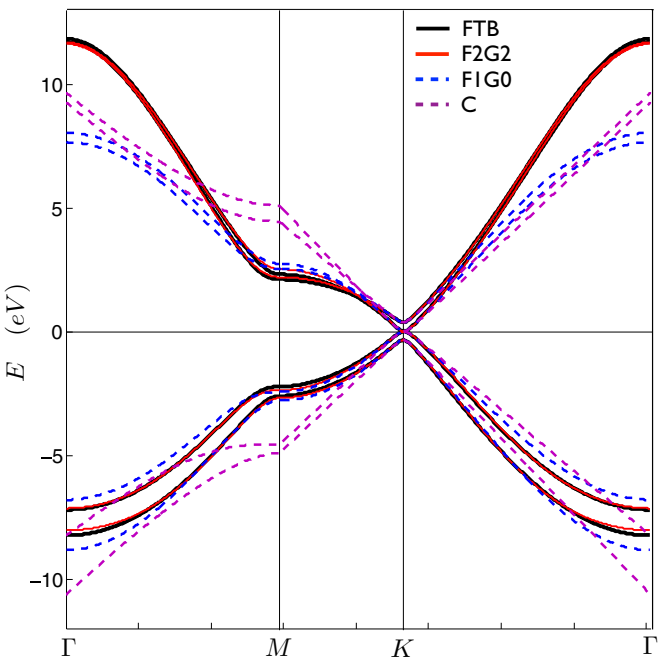

FIG. 8. (Color online) Comparison of the full tight-binding bands (FTB) as presented in Sec. II, and the simplified models presented in Sec. III consisting of the continuum model (C), the simplified tight-binding models with a single f_1 structure factor (F1G0), and with structure factors up to f_2 and g_2 (F2G2). We can observe that the simplest models C, F1G0 have substantial deviations away from the Dirac point, whereas F2G2 provides a good compromise between simplicity and accuracy.

TABLE III. Comparison of the effective F1G0 tight-binding model (see text) parameters in the present work with corresponding values from the literature. Our results taken from Table I agree best with the graphite LDA data of Ref. [25], and are in reasonable agreement with experimental fits to Raman Ref. [7] and infrared data Refs. [8,9] in bilayer graphene. Other tight-binding models for bilayer graphene motivated by graphite SMW parameters have been implemented with parameter sign differences in a variety of combinations leading to incorrect band structures [5,6,22,23]. Many properties of bilayer graphene are only weakly influenced by these remote hopping terms.

TB	SWM here	SWM Ref. [5]	SWM Ref. [22]	Present (LDA)	Graphite Ref. [25]	Bilayer Ref. [7]	Bilayer Ref. [8]	Bilayer Ref. [9]
$t_0 = t_{AB,1}$	$-\gamma_0$	γ_0	$-\gamma_0$	-2.61	-2.598	-2.9	-3.0	-3.16
$t_1 = t'_{BA',0}$	γ_1	γ_1	γ_1	0.361	0.377	0.30	0.40	0.381
$t_2 = t'_{AA'',0}$	$\gamma_2/2$	$\gamma_2/2$			-0.007			
$t_3 = t_{AB',1}$	γ_3	γ_3	$-\gamma_3$	0.283	0.319	0.10	0.3	0.38
$t_4 = t_{AA',1}$	γ_4	$-\gamma_4$	γ_4	0.138	0.177	0.12	0.15	0.14
$t_5 = t'_{BB''0}$	$\gamma_5/2$	$\gamma_5/2$			0.018			
$\Delta' = t'_{BB0}$	$\Delta - \gamma_2 + \gamma_5$	$\Delta - \gamma_2 + \gamma_5$	$\Delta - \gamma_2 + \gamma_5$	0.015	0.024		0.018	0.022

tight-binding model. The tight-binding parameters used in the comparison with the SWM model are the same as those used for the single structure factor F1G0 Hamiltonian in Eqs. (17)–(22). We note that the nearest-neighbor interlayer hopping parameters in the tight-binding and SWM model are defined so that they differ by a sign. The positive sign normally used for γ_0 is consistent with our finding that the numerical value of t_0 is negative.

Applications of the SWM model to generate tight-binding parameters for bilayer graphene in the literature have been confused by variations in parameter signs [5,6,21–23], which lead to inconsistent predictions for fine band features near the Dirac point. (In Table III we compare to values used in the literature for graphite and for bilayer graphene.) In an effort to clarify the confusion we define the effective velocity parameters $\upsilon = -t_0\sqrt{3}a/2\hbar$, $\upsilon_3 = t_3\sqrt{3}a/2\hbar$, and $\upsilon_4 = t_4\sqrt{3}a/2\hbar$ so that all have positive values. The LDA band effective velocities read from Table I are $\upsilon = 8.45 \times 10^5$ m/s, $\upsilon_3 = 9.16 \times 10^4$ m/s, and $\upsilon_4 = 4.47 \times 10^4$ m/s. Recalling that the expansions near the Dirac points of the nearest-neighbor structure factor are (to linear order) $f_1(\mathbf{k}_D + \mathbf{q}) = \sqrt{3}a(-q_x + iq_y)/2\hbar$ and $f_1(-\mathbf{k}_D + \mathbf{q}) = \sqrt{3}a(q_x + iq_y)/2\hbar$, where $\mathbf{k}_D = (4\pi/3a, 0)$, we rewrite Eq. (14) using a notation similar to that in Refs. [21,22] by defining $\pi = \hbar(\xi q_x + iq_y) = \hbar q \exp(i\theta_{\mathbf{q}})$ and $\pi^\dagger = \hbar(\xi q_x - iq_y) = \hbar q \exp(-i\theta_{\mathbf{q}})$, where $\theta_{\mathbf{q}}$ is an angle measured counterclockwise from the positive x axis and $\xi = \pm 1$ near $\pm\mathbf{k}_D$:

$$H(\mathbf{k}) = \begin{pmatrix} 0 & \upsilon\pi^\dagger & -\upsilon_4\pi^\dagger & -\upsilon_3\pi \\ \upsilon\pi & \Delta' & t_1 & -\upsilon_4\pi^\dagger \\ -\upsilon_4\pi & t_1 & \Delta' & \upsilon\pi^\dagger \\ -\upsilon_3\pi^\dagger & -\upsilon_4\pi & \upsilon\pi & 0 \end{pmatrix}. \quad (26)$$

This Hamiltonian has a $-$ sign in front of the υ_3 term when compared to Eq. (30) of Ref. [22]. The correct choice of relative signs for weak hopping processes can be relevant to the shape of the bands at low energies. The negative sign of t_0 implies that intralayer bonding states have lower energy than the antibonding counterparts. The most relevant term for vertical tunneling t_1 has a positive sign. As shown in Fig. 9 the relative sign of t_1 and t_3 determines the orientation of the trigonal distortion and the positions of the band-crossing points in bilayer graphene. The correct sign choice ($t_1 > 0, t_3 > 0$) implies bands that are similar to those obtained with the incorrect choice $t_1 < 0, t_3 < 0$ [23,24], whereas the incorrect mixed sign choice $t_1 > 0, t_3 < 0$ introduces a 60° rotation [21,22]. Taking the relative signs of t_0 and t_1 to be positive [5,6] or negative [21–24] does not affect the trigonal warping orientation, but alters the way in which the t_4 term influences particle-hole symmetry breaking in the bands.

These parameter sign issues also influence small terms in the 2×2 low-energy Hamiltonian [21,22] often used to describe the low-energy bands. Below, we rewrite Eq. (38) of

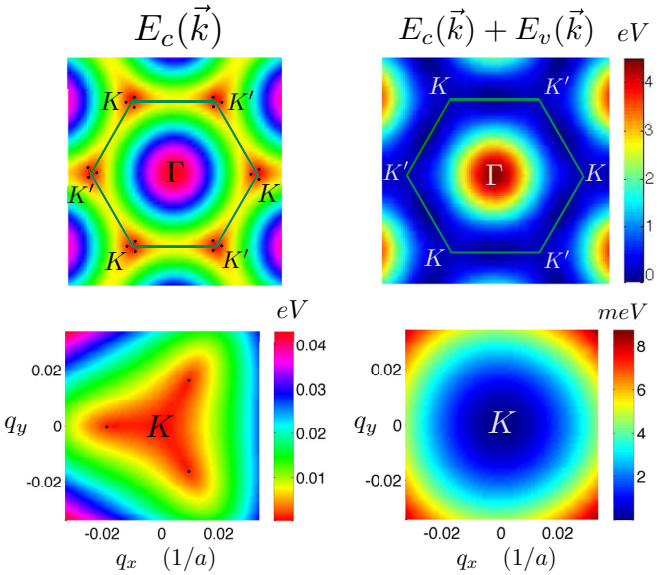

FIG. 9. (Color online) Two dimensional color scale plot of the LUMO band dispersion over the full Brillouin zone (top left) and near the $\mathbf{k}_D = (4\pi/3a, 0)$ Dirac point. The points at which the conduction and valence bands are degenerate are represented by black dots which lie at the vertices of a triangle. *Right panel:* Particle-hole symmetry breaking illustrated by plotting the sum of the LUMO (lowest conduction) and HOMO (highest valence) band energies $[E_c(\mathbf{k}) + E_v(\mathbf{k})]$. The main contribution comes from the AA' and BB' hopping processes as explained in the main text.

Ref. [22] (in the absence of an electric field between the layers) with the sign of the t_3 term corrected:

$$\begin{aligned}
\hat{H}_2 &= \hat{h}_0 + \hat{h}_3 + \hat{h}_4 + \hat{h}_\Delta, \\
\hat{h}_0 &= -\frac{v^2}{t_1}\begin{pmatrix} 0 & (\pi^\dagger)^2 \\ \pi^2 & 0 \end{pmatrix}, \\
\hat{h}_3 &= -v_3\begin{pmatrix} 0 & \pi \\ \pi^\dagger & 0 \end{pmatrix} + \frac{v_3 a}{4\sqrt{3}\hbar}\begin{pmatrix} 0 & (\pi^\dagger)^2 \\ -\pi^2 & 0 \end{pmatrix}, \\
\hat{h}_4 &= \frac{2vv_4}{t_1}\begin{pmatrix} \pi^\dagger\pi & 0 \\ 0 & \pi\pi^\dagger \end{pmatrix}, \\
\hat{h}_\Delta &= \frac{\Delta' v^2}{t_1'^2}\begin{pmatrix} \pi^\dagger\pi & 0 \\ 0 & \pi\pi^\dagger \end{pmatrix}.
\end{aligned} \tag{27}$$

The effective mass parameter $m = t_1/2v^2$ takes the value of $\sim 0.044 m_e$ when calculated from LDA bands. At K ($\xi = 1$) retaining only the term linear in $p = \hbar q$ for the trigonal warping gives the eigenenergies

$$\begin{aligned}
E_\pm &= \pm\left|\frac{v^2}{t_1}p^2\exp(-2i\theta_{\mathbf{q}}) + v_3 p\,\exp(i\theta_{\mathbf{q}})\right| \\
&= \pm\left|\frac{v^2}{t_1}p^2 + v_3 p\,\exp(i3\theta_{\mathbf{q}})\right|.
\end{aligned} \tag{28}$$

From this expression we can see how the relative signs of t_1 and t_3 determine the orientation of the degeneracy-point triangle. When $p = v_3 t_1/v^2$, the eigenvalues vanish for $\exp(i3\theta_{\mathbf{q}}) = -1$, i.e., when $\theta = \pi, \pm\pi/3$ as illustrated in Fig. 9. From the above equation we can also see that the sign of the particle-hole symmetry breaking changes with the signs of t_0, t_1, and t_4 parameters. Regarding particle-hole symmetry breaking we can see from Eqs. (27) that the leading coefficient of the parabolic term $2\hbar^2 vv_4/t_1 \sim 9$ eVÅ^2 due to the t_4 is far greater than the intralayer second order expansion terms in Eq. (16) $C'_{AA,2}, C'_{BB,2} \sim -0.2$ eVÅ^2 from Table I and indicates dominance of the interlayer coupling in defining the particle-hole symmetry breaking near the Dirac point.

V. SUMMARY AND CONCLUSIONS

We have presented accurate tight-binding models for AB stacked bilayer graphene based on maximally localized Wannier functions that can capture the band structure in the entire Brillouin zone and near the Dirac point. The models we have presented using orthogonal localized basis sets are able to provide a different insight with respect to earlier tight-binding models for bilayer graphene that use nonorthogonal localized orbitals with a finite overlap between neighboring sites. Our full tight-binding model that includes up to 17 in-plane distant hopping terms is able to reproduce almost exactly the LDA bands in the whole Brillouin zone. Effective models can be devised with fewer renormalized parameters using fewer structure factors that provide simpler models that remain accurate near the Dirac points. This recipe can be used systematically to build tight-binding models with improved description of the bands in the whole Brillouin zone but using fewer parameters. We specifically describe a five parameter model analogous to the SWM model of graphene, and a model with fifteen parameters that includes up to f_2 and g_2 structure factors and offers an excellent compromise between simplicity and achieved accuracy. Our *ab initio* approach has allowed us to assess the range of the microscopic hopping processes in graphene based systems. The parameters in SWM-type models are more correctly interpreted as effective hopping parameters that reproduce the bands near Dirac points.

We note that LDA band parameters differ from phenomenological values in part because the experiments which determine the latter are often influenced by many-body effects. For example, the effective intralayer nearest-neighbor hopping parameter is $|t_{AB1}| \sim 2.6$ eV for each graphene layer, similar to its value in single-layer graphene and corresponding to a velocity of $v \sim 0.84 \times 10^6$ m/s. The value is $10\% \sim 20\%$ smaller than $|t_{AB1}| \sim 3$ eV commonly extracted from fits to experiments. This renormalization of the Fermi velocity in single particle models that generally allows a better fit to experiments can be included as an *ad hoc* correction in the nearest-neighbor hopping term increasing the magnitude of the t_{AB1} term by 0.4 eV, that reproduces values similar to GW calculations [26]. We ascribe this shift to the quasiparticle velocity renormalization due to nonlocal exchange [27–29] that is not captured by the LDA. The strength of this renormalization depends on the carrier density and the dielectric environment [30–32], among other variable parameters, so it should be accounted for separately as necessary and not really be incorporated into a universally applicable band structure model. At very low carrier density this physics can in principle lead to broken symmetry states both in bilayers [23,33] and in ABC trilayers [24,34].

The most important interlayer coupling effects are controlled by the effective BA' coupling of ~ 360 meV whose structure factor does not vanish near the Dirac point, unlike the interlayer coupling mediated through terms linking AA'/BB' with an effective strength of ~ 140 meV each, that accounts for most of the particle-hole symmetry breaking near the Dirac points represented in Fig. 9, and terms coupling AB' sites in the order of ~ 280 meV responsible for trigonal warping. The interlayer coupling leads to a small modification in the intralayer Hamiltonian that introduces a small site potential difference of ~ 15 meV between A and B (or equivalently A' and B' sites) that influences the position of the higher-energy π bands. The models we have presented provide a useful reference for accurately modeling the first principles LDA electronic structure of bilayer graphene.

ACKNOWLEDGMENTS

This work was supported by the US Department of Energy Division of Materials Sciences and Engineering under Grant No. DE-FG03-02ER45958, by Welch Foundation Grant No. TBF1473, and by the National Science Foundation under Grant No. DMR-1122603. J.J. was partially supported by the National Research Foundation of Singapore under its Fellowship program (NRF-NRFF2012-01). We gratefully acknowledge the assistance and the computational resources provided by the Texas Advanced Computing Center. We thank the developers of WANNIER90 and QUANTUM ESPRESSO for making these tools freely available.

APPENDIX A: DEFINITIONS USED IN THE MAIN TEXT

We define our Wannier functions so that the Bloch states are given by

$$|\psi_{\mathbf{k}\alpha}\rangle = \frac{1}{\sqrt{N}}\sum_{\mathbf{R}} e^{i\mathbf{k}(R+\tau_\alpha)}|\mathbf{R}+\tau_\alpha\rangle, \tag{A1}$$

where the label α is the sublattice, τ_α is the position of the sublattice with respect to the lattice vectors $\mathbf{R}$, and $|\mathbf{R}+\tau_\alpha\rangle$ is a localized Wannier function. The Hamiltonian matrix elements are related with the Wannier representation hopping amplitudes through

$$\begin{aligned} H_{\alpha\beta}(\mathbf{k}) &= \langle\psi_{\mathbf{k}\alpha}|H|\psi_{\mathbf{k}\beta}\rangle \\ &= \frac{1}{N}\sum_{\mathbf{R}\mathbf{R}'} e^{i\mathbf{k}(\mathbf{R}'-\mathbf{R})}t_{\alpha\beta}(\mathbf{R}-\mathbf{R}'), \end{aligned} \tag{A2}$$

where

$$t_{\alpha\beta}(\mathbf{R}-\mathbf{R}') = \langle\mathbf{R}+\tau_\alpha|H|\mathbf{R}'+\tau'_\beta\rangle \tag{A3}$$

is the tunneling from β to α sublattice sites located respectively at $\mathbf{R}'+\tau'_\beta$ and $\mathbf{R}+\tau_\alpha$. We have chosen a coordinate system for the lattice vectors in which the honeycomb's Bravais lattice has primitive vectors

$$\vec{a}_1 = a(1,0), \quad \vec{a}_2 = a\left(\frac{1}{2},\frac{\sqrt{3}}{2}\right), \tag{A4}$$

where $a = 2.46$ Å is the lattice constant of graphene. The reciprocal lattice vectors are then

$$\vec{b}_1 = \frac{4\pi}{\sqrt{3}a}\left(\frac{\sqrt{3}}{2},-\frac{1}{2}\right), \quad \vec{b}_2 = \frac{4\pi}{\sqrt{3}a}(0,1). \tag{A5}$$

We choose $\tau_A = (0,0)$ and $\tau_B = (0,a/\sqrt{3})$ for the sublattices of the bottom layer and $\tau_{A'} = (0,a/\sqrt{3})$ and $\tau_{B'} = (0,2a/\sqrt{3})$ for the sublattices of the top layer. For convenience of the readers we list here the structure factors up to $n = 2$ from the complete list offered in Tables III and IV of Ref. [16]. For f_n we have

$$\begin{aligned} f_1(\mathbf{k}) &= e^{i\frac{k_y a}{\sqrt{3}}} + 2e^{-i\frac{k_y a}{2\sqrt{3}}}\cos\left(\frac{k_x a}{2}\right), \\ f_2(\mathbf{k}) &= e^{-i\frac{k_y 2a}{\sqrt{3}}} + 2e^{i\frac{k_y a}{\sqrt{3}}}\cos(k_x a), \end{aligned} \tag{A6}$$

and for g_n we have

$$\begin{aligned} g_0 &= 1, \\ g_1(\mathbf{k}) &= 2\cos(k_x a) + 4\cos\left(\frac{k_y\sqrt{3}a}{2}\right)\cos\left(\frac{k_x a}{2}\right), \\ g_2(\mathbf{k}) &= 2\cos(k_y\sqrt{3}a) + 4\cos\left(\frac{k_y\sqrt{3}a}{2}\right)\cos\left(\frac{k_x 3a}{2}\right). \end{aligned} \tag{A7}$$

APPENDIX B: TABLES FOR THE PARAMETERS IN THE FULL TIGHT-BINDING MODEL

In this Appendix we list in Tables IV and V the distant tight-binding hopping parameters used for AB stacked bilayer graphene, associated with the $f_n(\mathbf{k})$ and $g_n(\mathbf{k})$ terms calculated using 30×30 k-point sampling density.

TABLE IV. Hopping amplitudes in eV units obtained in the LDA calculations associated to $f_n(\mathbf{k})$ structure factors connecting AB, AB', and AA'.

n	m	N^0	d_n/a	t_{ABn}	$t_{AA'n}$	$t_{AB'n}$
1	1	3	$\frac{1}{\sqrt{3}}$	−3.010	0.09244	0.13912
2	3	3	$\frac{2}{\sqrt{3}}$	−0.2387	−0.01803	−0.04753
3	4	6	$\sqrt{\frac{7}{3}}$	0.01900	−0.00068	−0.00108
4	7	6	$\sqrt{\frac{13}{3}}$	−0.01165	0.00181	0.00613
5	8	3	$\frac{4}{\sqrt{3}}$	−0.01167	0.00029	−0.00016
6	9	6	$\sqrt{\frac{19}{3}}$	−0.00824	−0.00019	−0.00152
7	11	3	$\frac{5}{\sqrt{3}}$	0.00386	−0.00079	−0.00163
8	13	6	$\sqrt{\frac{28}{3}}$	0.00250	0.00007	−0.00152
9	14	6	$\sqrt{\frac{31}{3}}$	0.00224	−0.00010	0.00075
10	16	6	$\sqrt{\frac{37}{3}}$	−0.00012	0.00052	0.00062

APPENDIX C: RELATIONSHIP BETWEEN SWM AND THE EFFECTIVE TIGHT-BINDING MODEL PARAMETERS

In the following we paraphrase the analysis to compare the SWM model and the tight-binding model for graphite presented in Ref. [5] particularized for bilayer graphene and the simplified tight-binding model we proposed in Eqs. (17)–(22). The SWM model for a bilayer graphene is simplified because $\gamma_2 = \gamma_5 = 0$ and the absence of the dispersion along the z axis resulting in the Hamiltonian

$$H_{\mathrm{SWM}} = \begin{pmatrix} E_1 & 0 & H_{13} & H_{13}^* \\ 0 & E_2 & H_{23} & -H_{23}^* \\ H_{13}^* & H_{23}^* & E_3 & H_{33} \\ H_{13} & -H_{23} & H_{33}^* & E_3 \end{pmatrix}, \tag{C1}$$

TABLE V. Hopping amplitudes in eV units obtained in the LDA calculations associated to $g_n(\mathbf{k})$ structure factors connecting AA, BB, and BA'. We have introduced small equal shifts in the site terms $t'_{\alpha\alpha,0}$ so that the $C'_{\alpha\alpha,0}$ obtained from the truncated sum matches the values adopted for the position of the Fermi energy in Table I.

n	m	N^0	d_n/a	t'_{AAn}	t'_{BBn}	$t'_{BA'n}$
0	0	1	0	0.4295	0.4506	0.3310
1	2	6	1	0.22349	0.2260	−0.01016
2	5	3	$\sqrt{3}$	0.03692	0.03741	0.00049
2*	5*	3	$\sqrt{3}$	0.03692	0.03741	0.00271
3	6	6	2	−0.00253	−0.00163	0.00407
4	10	6	$\sqrt{7}$	0.00076	0.00045	−0.00266
4*	10*	6	$\sqrt{7}$	0.00076	0.00045	−0.00049
5	12	6	3	0.00327	0.00292	−0.00180
6	15	3	$\frac{6}{\sqrt{3}}$	−0.00085	−0.00056	0.00222
6*	15*	3	$\frac{6}{\sqrt{3}}$	−0.00085	−0.00056	0.00015
7	17	6	$\sqrt{\frac{39}{3}}$	−0.00031	−0.00004	0.00143
7*	17*	6	$\sqrt{\frac{39}{3}}$	−0.00031	−0.00004	0.00034

where for a bilayer graphene $\Gamma = 2$ we have

$$E_1 = 2\gamma_1 + \Delta, \tag{C2}$$

$$E_2 = -2\gamma_1 + \Delta, \tag{C3}$$

$$E_3 = 0, \tag{C4}$$

$$H_{13} = \frac{1}{\sqrt{2}}(-\gamma_0 + 2\gamma_4)\sigma \exp(i\alpha), \tag{C5}$$

$$H_{33} = 2\gamma_3\sigma \exp(i\alpha), \tag{C6}$$

where $\sigma = \sqrt{3}aq/2$ with q measured from the Dirac point and $\alpha = \arctan(-q_x/q_y)$ is the angle measured from the q_y axis. We will compare with the eigenvalues obtained from the continuum Hamiltonian in Eq. (14). Right at the Dirac point where $\sigma = 0$ and $F_{\alpha\beta}(\mathbf{k}_D) = 0$ the four eigenvalues of the SWM Hamiltonian are E_1, E_2 and the doubly degenerate E_3. Comparing with the four eigenvalues of the tight-binding Hamiltonian we can conclude that

$$\gamma_1 = t_1, \tag{C7}$$

$$\Delta = \Delta'. \tag{C8}$$

The eigenvalues along the ΓK line from the SWM bilayer graphene model are given by

$$E_{1,2} = \frac{\Delta}{2} + \gamma_3\sigma + \gamma_1 \pm \frac{1}{2}\sqrt{C + D}, \tag{C9}$$

$$E_{3,4} = \frac{\Delta}{2} - \gamma_3\sigma - \gamma_1 \pm \frac{1}{2}\sqrt{C + D}, \tag{C10}$$

where

$$C = \Delta^2 + 4\gamma_3^2\sigma^2 - 8\gamma_3\gamma_1\sigma \tag{C11}$$

$$+ 4\gamma_1^2 + 4\gamma_0^2\sigma^2 + 16\gamma_4^2\sigma^2, \tag{C12}$$

$$D = 4\gamma_1\Delta - 4\Delta\gamma_3\sigma - 16\gamma_0\gamma_4\sigma^2. \tag{C13}$$

This is to be compared with the four eigenvalues of the effective continuum model whose eigenvalues are

$$E'_{1,2} = \frac{\Delta'}{2} + t_3\sigma + t_1 \pm \frac{1}{2}\sqrt{C' + D'}, \tag{C14}$$

$$E'_{3,4} = \frac{\Delta'}{2} - t_3\sigma - t_1 \pm \frac{1}{2}\sqrt{C' - D'}, \tag{C15}$$

where

$$C' = \Delta'^2 + 4t_3^2\sigma^2 - 8t_3t_1\sigma \tag{C16}$$

$$+ 4t_1^2 + 4t_0^2\sigma^2 + 16t_4^2\sigma^2, \tag{C17}$$

$$D' = 4t_1\Delta - 4\Delta t_3\sigma + 16t_0t_4\sigma^2. \tag{C18}$$

When we compare Eqs. (C9)–(C13) from SWM model and Eqs. (C14)–(C18) formally there is only one difference in the sign of the last term of Eq. (C18) that would lead to $-\gamma_0\gamma_4 = t_0t_4$ if we want all the eigenvalues to remain the same. The physical choice of signs consistent with our calculations is $t_0 = -\gamma_0$ and $t_4 = \gamma_4$.

[1] P. R. Wallace, Phys. Rev. **71**, 622 (1947).

[2] J. C. Slonczewski and P. R. Weiss, Phys. Rev. **109**, 272 (1958); J. C. Slonczewski, Ph.D. thesis, Rutgers University, 1955; J. W. McClure, Phys. Rev. **108**, 612 (1957).

[3] R. C. Tatar and S. Rabii, Phys. Rev. B **25**, 4126 (1982).

[4] H. Min and A. H. MacDonald, Phys. Rev B **77**, 155416 (2008).

[5] B. Partoens and F. M. Peeters, Phys. Rev. B **74**, 075404 (2006).

[6] J. Nilsson, A. H. Castro Neto, F. Guinea, and N. M. R. Peres, Phys. Rev. B **78**, 045405 (2008); E. V. Castro, K. S. Novoselov, S. V. Morozov, N. M. R. Peres, J. M. B. Lopes dos Santos, J. Nilsson, F. Guinea, A. K. Geim, and A. H. Castro Neto, J. Phys.: Condens. Matter **22**, 175503 (2010).

[7] L. M. Malard, J. Nilsson, D. C. Elias, J. C. Brant, F. Plentz, E. S. Alves, A. H. Castro Neto, and M. A. Pimenta, Phys. Rev. B **76**, 201401 (2007).

[8] L. M. Zhang, Z. Q. Li, D. N. Basov, M. M. Fogler, Z. Hao, and M. C. Martin, Phys. Rev. B **78**, 235408 (2008).

[9] A. B. Kuzmenko, I. Crassee, D. van der Marel, P. Blake, and K. S. Novoselov, Phys. Rev. B **80**, 165406 (2009).

[10] H. Min, B. Sahu, S. K. Banerjee, and A. H. MacDonald, Phys. Rev. B **75**, 155115 (2007).

[11] S. Latil and L. Henrard, Phys. Rev. Lett. **97**, 036803 (2006); M. Aoki and H. Amawashi, Solid State Commun. **142**, 123 (2007); P. Gava, M. Lazzeri, A. M. Saitta, and F. Mauri, Phys. Rev. B **79**, 165431 (2009).

[12] N. Marzari, A. A. Mostofi, J. R. Yates, I. Souza, and D. Vanderbilt, Rev. Mod. Phys. **84**, 1419 (2012).

[13] R. Saito, G. Dresselhaus, and M. S. Dresselhaus, *Physical Properties of Carbon Nanotubes* (Imperial, London, 1998).

[14] In single-layer graphene the coupling between σ and π bands vanishes by mirror-plane symmetry. Coupling is present in bilayers, although the hopping amplitude between a p_z orbitals at a carbon site and a neighboring bonding σ orbital is smaller than 0.1 eV in magnitude. Considering the large separation in energy over 10 eV between the p_z and the σ orbitals this weak coupling implies negligibly small mixing between the two types of orbitals.

[15] G. Onida, L. Reining, and A. Rubio, Rev. Mod. Phys. **74**, 601 (2002).

[16] J. Jung and A. H. MacDonald, Phys. Rev. B **87**, 195450 (2013).

[17] P. Giannozzi, S. Baroni, N. Bonini, M. Calandra, R. Car, C. Cavazzoni, D. Ceresoli, G. L. Chiarotti, M. Cococcioni, I. Dabo, A. Dal Corso, S. Fabris, G. Fratesi, S. de Gironcoli, R. Gebauer, U. Gerstmann, C. Gougoussis, A. Kokalj, M. Lazzeri, L. Martin-Samos, N. Marzari, F. Mauri, R. Mazzarello, S. Paolini, A. Pasquarello, L. Paulatto, C. Sbraccia, S. Scandolo, G. Sclauzero, A. P. Seitsonen, A. Smogunov, P. Umari, and R. M. Wentzcovitch, J. Phys.: Condens. Matter **21**, 395502 (2009).

[18] A. A. Mostofi, J. R. Yates, Y.-S. Lee, I. Souza, D. Vanderbilt, and N. Marzari, Comput. Phys. Commun. **178**, 685 (2008).

[19] J. P. Perdew and A. Zunger, Phys. Rev. B **23**, 5048 (1981).
[20] W. Kohn, Rev. Mod. Phys. **71**, 1253 (1999).
[21] E. McCann and V. I. Fal'ko, Phys. Rev. Lett. **96**, 086805 (2006).
[22] E. McCann and M. Koshino, Rep. Prog. Phys. **76**, 056503 (2013).
[23] J. Jung, F. Zhang, and A. H. MacDonald, Phys. Rev. B **83**, 115408 (2011).
[24] J. Jung and A. H. MacDonald, Phys. Rev. B **88**, 075408 (2013).
[25] J.-C. Charlier, X. Gonze, and J.-P. Michenaud, Phys. Rev. B **43**, 4579 (1991).
[26] A. Grüneis, C. Attaccalite, L. Wirtz, H. Shiozawa, R. Saito, T. Pichler, and A. Rubio, Phys. Rev. B **78**, 205425 (2008); A. Gruneis, C. Attaccalite, A. Rubio, D. V. Vyalikh, S. L. Molodtsov, J. Fink, R. Follath, W. Eberhardt, B. Buchner, and T. Pichler, *ibid.* **79**, 205106 (2009); **80**, 075431 (2009).
[27] J. Jung and A. H. MacDonald, Phys. Rev. B **84**, 085446 (2011).
[28] J. Gonzalez, F. Guinea, and M. A. H. Vozmediano, Phys. Rev. B **59**, R2474 (1999); Phys. Rev. Lett. **77**, 3589 (1996); Nucl. Phys. B **424**, 595 (1994); J. Low Temp. Phys. **99**, 287 (1995); F. Guinea, A. H. Castro Neto, and N. M. R. Peres, Eur. Phys. J. Special Topics **148**, 117 (2007).
[29] D. C. Elias, R. V. Gorbachev, A. S. Mayorov, S. V. Morozov, A. A. Zhukov, P. Blake, K. S. Novoselov, A. K. Geim, and F. Guinea, Nature Phys. **7**, 701 (2011).
[30] Y. Barlas, T. Pereg-Barnea, M. Polini, R. Asgari, and A. H. MacDonald, Phys. Rev. Lett. **98**, 236601 (2007).
[31] G. Borghi, M. Polini, R. Asgari, and A. H. MacDonald, Solid State Commun. **149**, 1117 (2009); A. Principi, M. Polini, R. Asgari, and A. H. MacDonald, *ibid.* **152**, 1456 (2012).
[32] J. Jung, M. Polini, and A. H. MacDonald, arXiv:1111.1765.
[33] H. Min, G. Borghi, M. Polini, and A. H. MacDonald, Phys. Rev. B **77**, 041407(R) (2008); F. Zhang, J. Jung, G. A. Fiete, Q. Niu, and A. H. MacDonald, Phys. Rev. Lett. **106**, 156801 (2011); F. Zhang, H. Min, M. Polini, and A. H. MacDonald, Phys. Rev. B **81**, 041402(R) (2010); R. Nandkishore and L. Levitov, Phys. Rev. Lett. **104**, 156803 (2010); Phys. Rev. B **82**, 115124 (2010); **82**, 115431 (2010); T. C. Lang, Z. Y. Meng, M. M. Scherer, S. Uebelacker, F. F. Assaad, A. Muramatsu, C. Honerkamp, and S. Wessel, Phys. Rev. Lett. **109**, 126402 (2012); F. Zhang, H. Min, and A. H. MacDonald, Phys. Rev. B **86**, 155128 (2012); E. V. Gorbar, V. P. Gusynin, V. A. Miransky, and I. A. Shovkovy, *ibid.* **85**, 235460 (2012); M. Kharitonov, *ibid.* **86**, 195435 (2012); G. M. Rutter, S. Jung, N. N. Klimov, D. B. Newell, N. B. Zhitenev, and J. A. Stroscio, Nature Phys. **7**, 649 (2011); O. Vafek and K. Yang, Phys. Rev. B **81**, 041401(R) (2010); O. Vafek, *ibid.* **82**, 205106 (2010); R. E. Throckmorton and O. Vafek, *ibid.* **86**, 115447 (2012); V. Cvetkovic, R. E. Throckmorton, and O. Vafek, *ibid.* **86**, 075467 (2012); M. M. Scherer, S. Uebelacker, and C. Honerkamp, *ibid.* **85**, 235408 (2012); Y. Lemonik, I. L. Aleiner, C. Toke, and V. I. Fal'ko, *ibid.* **82**, 201408(R) (2010); Y. Lemonik, I. L. Aleiner, and V. I. Fal'ko, *ibid.* **85**, 245451 (2012); B. Feldman, J. Martin, and A. Yacoby, Nature Phys. **5**, 889 (2009); R. T. Weitz, M. T. Allen, B. E. Feldman, J. Martin, and A. Yacoby, Science **330**, 812 (2010); J. Velasco, Jr., L. Jing, W. Bao, Y. Lee, P. Kratz, V. Aji, M. Bockrath, C. N. Lau, C. Varma, R. Stillwell, D. Smirnov, F. Zhang, J. Jung, and A. H. MacDonald, Nat. Nanotech. **7**, 156 (2012); W. Bao, J. Velasco, Jr., F. Zhang, L. Jing, B. Standley, D. Smirnov, M. Bockrath, A. H. MacDonald, and C. N. Lau, Proc. Natl. Acad. Sci. USA **109**, 10802 (2012); F. Freitag, M. Weiss, R. Maurand, J. Trbovic, and C. Schönenberger, Solid State Commun. **152**, 2053 (2012); F. Freitag, J. Trbovic, M. Weiss, and C. Schönenberger, Phys. Rev. Lett. **108**, 076602 (2012).
[34] W. Bao, L. Jing, Y. Lee, J. Velasco, Jr., P. Kratz, D. Tran, B. Standley, M. Aykol, S. B. Cronin, D. Smirnov, M. Koshino, E. McCann, M. Bockrath, and C. N. Lau, Nat. Phys. **7**, 948 (2011); M. Nakamura and L. Hirasawa, Phys. Rev. B **77**, 045429 (2008); D.-H. Xu, J. Yuan, Z.-J. Yao, Y. Zhou, J.-H. Gao, and F.-C. Zhang, *ibid.* **86**, 201404(R) (2012); M. M. Scherer, S. Uebelacker, D. D. Scherer, and C. Honerkamp, *ibid.* **86**, 155415 (2012); V. Cvetkovic and O. Vafek, arXiv:1210.4923; R. Olsen, R. van Gelderen, and C. M. Smith, Phys. Rev. B **87**, 115414 (2013).